

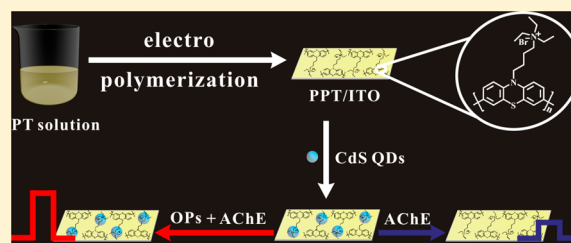
# Electropolymerization-Induced Positively Charged Phenothiazine Polymer Photoelectrode for Highly Sensitive Photoelectrochemical Biosensing

Jiao Wang, Wenxin Lv, Jiahui Wu, Haiyin Li,\* and Feng Li\*<sup>ID</sup>

College of Chemistry and Pharmaceutical Sciences, Qingdao Agricultural University, Qingdao 266109, People's Republic of China

## S Supporting Information

**ABSTRACT:** Exploring the fabrication of an electrode with high photoelectric conversion efficiency and abundant functional groups for ideal photoelectrochemical (PEC) sensor development is highly urgent but faces a significant challenge. Herein we report an electropolymerization strategy for the preparation of phenothiazine polymeric film on an indium tin oxide (ITO) surface (PPT/ITO), within only a few seconds, and monomers. The fabricated PPT/ITO electrode possessed excellent stability and abundant quaternary ammonium salt groups for developing a highly sensitive PEC sensor through electrostatic binding with negatively charged materials. In this context, a CdS QDs-functionalized PPT/ITO electrode (CdS/PPT/ITO) was proposed and applied to the analysis of chlorpyrifos, used as a model target organophosphorous pesticide (OP). The thiocholine generated from acetylcholinesterase (AChE)-induced catalyzed hydrolysis of acetylthiocholine (ATCh) efficiently directed CdS QDs away from PPT/ITO via electrostatic repulsion, subsequently decreasing PEC current, whereas chlorpyrifos prohibited the generation of thiocholine through inhibiting AChE activity. As compared to the case where chlorpyrifos is absent, significantly enhanced PEC current is determined and is proportional to chlorpyrifos amounts. Thus, the developed CdS/PPT/ITO-based PEC sensor achieved excellent chlorpyrifos biosensing with improved sensitivity down to approximately ng/mL level with good specificity. We envision the proposed strategy will provide a new path to conveniently fabricate photoelectrodes possessing high performance, which will have more useful applications in PEC sensing.



Advances in photoelectrochemical (PEC) sensing systems over the past few years has significantly effected the diagnosis of various diseases on the basis of electrochemistry and photochemistry.<sup>1–5</sup> In PEC systems, electrodes can convert light into current and are regarded as the most critical components, thus attracting substantial attention to explore new manufacturing technology and architecture. Despite recent progress, the design and development of electrodes are still dependent on the drop-coating method,<sup>6–8</sup> which easily leads to unrepeatability and instability, subsequently precluding PEC sensing applications. In addition, diverse materials such as TiO<sub>2</sub>,<sup>9,10</sup> ZnO,<sup>11,12</sup> and CdS<sup>13,14</sup> have been used as photoactive elements for development of photoelectrodes, but their applications are quite restricted as a result of the lack of functional groups. Therefore, PEC electrodes are currently facing two great challenges: poor manufacturing technology and lack of functionality, which force us to address them for PEC sensing applications.

Conjugated polymers, which have a broad light absorption range, tunable redox active properties, and abundant functional groups, are recognized as ideal candidates to fabricate photoelectrodes.<sup>15–18</sup> For example, 1,4-diethynylbenzene polymer has been used as a functional material for photoelectrochemical water reduction.<sup>17</sup> Despite wide investigations, these aromatic polymers are currently prepared through chemical polymerizations,<sup>19</sup> such as the Suzuki reaction,<sup>20</sup>

Heck reaction,<sup>21</sup> Wittig–Horner reaction,<sup>22</sup> and oxidative reaction,<sup>23</sup> and are limited by the following obstacles: (1) Expensive precious metal catalysts are required in the polymerization process;<sup>20</sup> (2) the prepared polymers exhibit poor repeatability and solubility because of the rigid chains and strong interaction force, making it difficult to form a film or layer on the electrode surface;<sup>16</sup> (3) the process is both tedious and complicated and produces large amounts of waste. In this context, it is highly desirable to propose an effective and practical film-forming approach for conjugated polymers for fabricating the photoelectrodes.

Recent studies demonstrate that electropolymerization can be used as an alternative tool for fabricating conjugated polymer-modified electrodes without the need for any catalyst and template.<sup>24,25</sup> Regarding the exceptional processability of conducting polymers obtained from electropolymerization, substantial progress has been made toward the development of electrodes from various aromatic monomers via electropolymerization.<sup>26,27</sup> Among these monomers, phenothiazine and its derivatives, comprising electron-rich N and S, are recognized as highly popular building units for fabricating electrodes due to the reversible radical cation formation and

Received: July 21, 2019

Accepted: September 27, 2019

Published: September 27, 2019



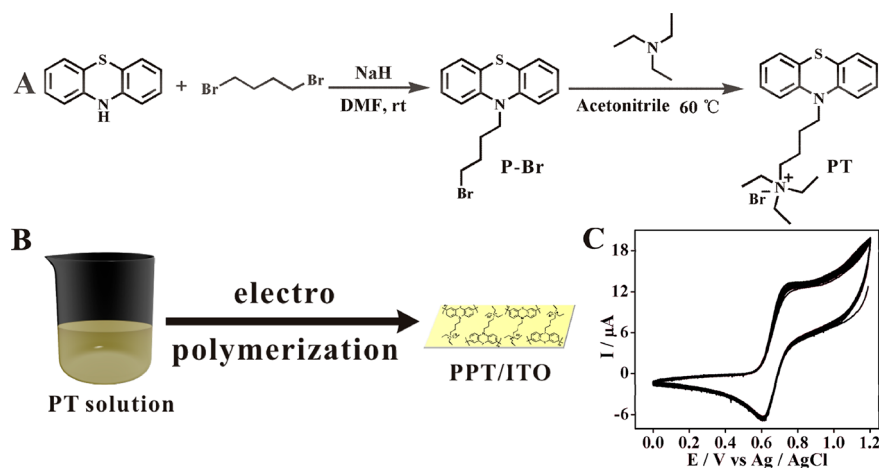


**Figure 1.** (A) Synthetic route for monomer PT. (B) Diagram of fabrication of PPT/ITO via CV electropolymerization. (C) CV curves (1st to 20th cycles) of PT solution in acetonitrile in the presence of NaClO<sub>4</sub> electrolyte at 25 °C with a scan rate of 0.1 V s<sup>-1</sup>.

tunable redox property.<sup>28–31</sup> The inherent features enable development of polyphenothiazine-modified electrodes via electropolymerization for applications in solar cells.<sup>32–34</sup> If we introduce phenothiazine polymers into photoelectrodes for developing PEC sensors via electropolymerization, such sensors could efficiently address the challenge of film formation for sensitive and accurate determination of various target biomolecules. However, as far as we are concerned, these fabricated electrodes still lack functional groups, being adverse to modification with functional substances, and no effort has been devoted to exploring such electrodes for PEC sensing.

Herein, by making full use of organic coupling and electropolymerization reactions, a phenothiazine polymer-modified electrode (PPT/ITO) was successfully fabricated with abundant quaternary ammonium salt groups on the surface. On the basis of positive groups of the fabricated PPT/ITO, a facile conjugation strategy for devising the PEC sensor was elaborately proposed based on electrostatic interaction. In the present study, the conjugation was applied for negatively charged CdS QDs, used as the model conjugates. Scanning electron microscopy (SEM), energy-dispersive spectrometry (EDS), X-ray photoelectron spectroscopy (XPS), PEC, and other characterizations depict that CdS QDs were effectively decorated on the PPT/ITO surface, and the amount of CdS QDs directly impacted the PEC current. We demonstrate that CdS/PPT/ITO is a promising acetylcholinesterase (AChE)-responsive PEC sensor for an organophosphorous pesticide (OP) assay. CdS/PPT/ITO displays high PEC current and, contrarily, exhibits relatively low PEC current in the presence of AChE. This decrease is caused by the wide separation of PPT/ITO and CdS QDs induced by thiocholine derived from AChE-catalyzed hydrolysis of acetylthiocholine (ATCh). When an OP is present in the system, AChE activity will be severely inhibited and then no thiocholine generated. As a result, the CdS QDs would be also compactly anchored on the PPT/ITO surface, subsequently hampering the PEC current decrease. Based on the variation of PEC current, sensitive detection of OP can be readily achieved.

## EXPERIMENTAL SECTION

**Preparation of Phenothiazine Monomer PT.** Phenothiazine (3.00 g, 0.015 mol), 1,4-dibromobutane (9.72 g, 0.045 mol), and NaH (0.72 g, 0.03 mol) were added into 30 mL of

*N,N*-dimethylformamide (DMF), and the solution was stirred for 12 h. Subsequently, the reaction solution was poured into ice–water and extracted with dichloromethane three times. The organic phase was dried using MgSO<sub>4</sub> and concentrated through rotary evaporation. Then intermediate P–Br was purified by column chromatography (silica gel, CH<sub>2</sub>Cl<sub>2</sub>/*n*-hexane 1/6) and dried in a vacuum at room temperature overnight.

Subsequently, the intermediate P–Br was added into 30 mL of acetonitrile, and the solution was stirred for 10 min to fully dissolve P–Br. A 2.0 mL amount of triethylamine was added into the mixture, and the resulting solution was permitted to react for 8.0 h at 60 °C under N<sub>2</sub> atmosphere. Then the end-product PT was obtained in the yield of 84.3% via recrystallization in toluene. <sup>1</sup>H NMR (500 MHz, CDCl<sub>3</sub>) δ (ppm): 1.25 (m, 9H), 1.52 (d, 2H), 1.73 (d, 2H), 3.06 (d, 2H), 3.24 (d, 2H), 3.28 (m, 6H), 6.68 (d, 2H), 6.75 (d, 2H), 6.91 (d, 2H), 6.99 (d, 2H). FT-IR (KBr) ν (cm<sup>-1</sup>): 3453, 2972, 1465, 1268, 1146, 1032, 758.

**Fabrication of the PPT/ITO Electrode via Electropolymerization.** An acetonitrile solution comprising 0.01 M PT and 0.2 M sodium perchlorate was used as electrolyte. The electropolymerization experiment was carried out in 5.0 mL of electrolyte solution with a potential of 0–1.5 V and scan rate of 0.1 V/s through using ITO (0.25 cm<sup>2</sup>), Ag/AgCl, and Pt wire as working electrode, reference electrode, and counter electrode, respectively. After different numbers of CV scans, the electrode was cleaned with acetonitrile to remove the adsorbed PT and sodium perchlorate and subsequently dried in vacuum to afford the PPT/ITO electrode.

**Fabrication of the CdS/PPT/ITO Electrode.** Twenty microliters of CdS QDs solution at different concentrations was dripped onto the PPT/ITO electrode and incubated for 30 min. After that, the electrode was rinsed with ultrapure water three times to remove the unreacted CdS QDs. The fabricated CdS/PPT/ITO electrode was placed in a humid condition at 4 °C for the subsequent determination.

**Detection of Chlorpyrifos Using the CdS/PPT/ITO-Based PEC Sensor.** The chlorpyrifos-triggered inhibition reaction was performed in 40 μL of 0.1 M PBS buffer (5 mM KCl, pH 7.4) containing 70 mU/mL AChE and chlorpyrifos at varying concentrations at 37 °C for 30 min. Subsequently, 160 μL of ATCh solution (0.375 mM) was added. The fabricated CdS/PPT/ITO electrode was immersed in 200 μL of this

reaction solution for 35 min. After being rinsed with ultrapure water three times, the photoelectrode was put into PBS buffer containing 0.001 M AA solution to carry out the PEC experiment under 430 nm light excitation.

## RESULTS AND DISCUSSION

**Design and Characterization of the PPT/ITO Electrode.** To guarantee the successful fabrication of the modified electrode with ideal characteristics, monomer PT was elaborately devised, which contained a phenothiazine moiety and quaternary ammonium salt groups, providing the units for electropolymerization and positively charged groups on the surface, respectively. The synthetic route for PT is illustrated in Figure 1A and mainly comprises an organic coupling reaction and quaterization in a yield of 84.3%.  $^1\text{H}$  NMR and FT-IR spectra were employed to confirm PT's molecular structure (Figure S1). Further, PT was used as raw material to fabricate the phenothiazine polymer-modified electrode (PPT/ITO) using cyclic voltammetry (CV) in acetonitrile solution comprising 0.20 M sodium perchlorate (Figure 1B). Figure 1C gives the CV information on PT up to 20 cycles. In the first CV scan, the onset potential of PT was located at 0.58 V, corresponding to the oxidation of the phenothiazine moiety. Along with the increased potential, the current elevated rapidly, strongly justifying the oxidation of more PT. Meanwhile, it should be noted that the current does not obviously increase when accompanied by an increase in the number of CV scans, which may be due to the poor conductivity induced by the increase in film thickness. Thus, one CV scan was applied in the preparation of the PPT/ITO electrode. This approach for direct fabrication of the PPT/ITO electrode is excellent because it only requires a few seconds and very few monomers.

To confirm the successful fabrication of the proposed electrode, CV characterizations were conducted in PBS buffer (Figure S2A). In comparison with the bare ITO electrode, PPT/ITO displayed a pair of well-defined redox peaks, with potentials that appeared at 0.60 and 0.55 V, respectively, corresponding well to the characteristic of phenothiazine polymer that was coated on the ITO surface. Meanwhile, PPT/ITO depicted a significant DPV peak current at 0.58 V compared with that of ITO (Figure S2B). Furthermore, from the electrochemical impedance spectroscopy (EIS) measurements, it can be clearly seen that the phenothiazine polymer caused the electron transfer resistance ( $R_{\text{et}}$ ) to significantly increase due to the weak conductivity of phenothiazine polymer (Figure S2C). In addition, some peaks in EDS and XPS curves appeared, corresponding to C, N, and S elements derived from phenothiazine (Figure S2D and Figure S2E). This information firmly indicated the effective deposition of phenothiazine polymeric film on the ITO electrode.

Subsequently, the electronic characteristics of phenothiazine polymer film were studied via the UV-vis absorption spectra (Figure S3). The phenothiazine film obtained from spin-coating demonstrated two absorption peaks located at 254 and 300 nm, respectively, which were attributable to different  $\pi-\pi^*$  transitions in the monomer. In contrast, phenothiazine polymer film presented red-shift peaks located at 277 and 307 nm, respectively, ascribed to the linkage of phenothiazine units. Under radiation from 365 nm light, PPT/ITO exported PEC current with an intensity of 33.17 nA. Changing the excitation wavelength to 430 nm reduced the current greatly (Figure S4), corresponding well to the UV-vis spectrum. Moreover, PPT/

ITO presented a smooth and compact surface morphology, which is important for the development of PEC sensors (Figure S5). Furthermore, the chemical stability of the PPT/ITO electrode was studied by dispersing it in a highly concentrated solution composed of  $\text{Na}_2\text{SO}_4$ , KCl,  $\text{Mg}(\text{NO}_3)_2$ , and  $\text{ZnCl}_2$  for 12 h. CV and EIS characterizations revealed that PPT/ITO retained the same peaks and conductivity as observed for untreated PPT/ITO (Figure S6).

**Development of the CdS/PPT/ITO Electrode.** The above-mentioned experimental information led us to explore the development of a functional heterojunction photoelectrode from PPT/ITO, which would exhibit excellent conduction. As is well-known, CdS QDs are one of the most used n-type semiconductors for the preparation of photoelectrodes with high photoelectric conversion efficiency because of low cost, excellent photophysical characters, uniform morphology, and large surface area and thus were applied as model conjugates to fabricate the photoelectrode. In the present study, CdS QDs with a  $\text{Cd}^{2+}$ -rich surface were prepared via a hydrothermal method by using sodium citrate as stabilizing agent.<sup>35</sup> TEM and zeta measurements demonstrated that the prepared CdS QDs depicted sphere morphology with a size of 4 nm in diameter (Figure S7A) and possessed a significant negative zeta potential ( $-20.10$  mV), justifying the distinguished water dispersibility and strong electrostatic interaction toward positively charged substances. In addition, CdS QDs show two absorption bands at 363 and 423 nm with a molar absorptivity of  $367000\text{ M}^{-1}\text{ cm}^{-1}$  and  $323300\text{ M}^{-1}\text{ cm}^{-1}$ , respectively, benefiting the highly efficient visible light photoexcitation (Figure S7B).

The diagram of interaction of PPT/ITO and CdS QDs is shown in Figure 2A. PPT/ITO has quaternary ammonium salt groups on the surface and thus can adsorb negatively charged CdS QDs to fabricate the heterojunction photoelectrode. As expected, PEC current gradually increased with an increase in the amount of CdS QDs from 0 to  $2.0\text{ }\mu\text{M}$  under 430 nm light irradiation due to the electrostatic adsorption (Figure 2B). However, when CdS QDs exceeded  $2.0\text{ }\mu\text{M}$ , no evident change

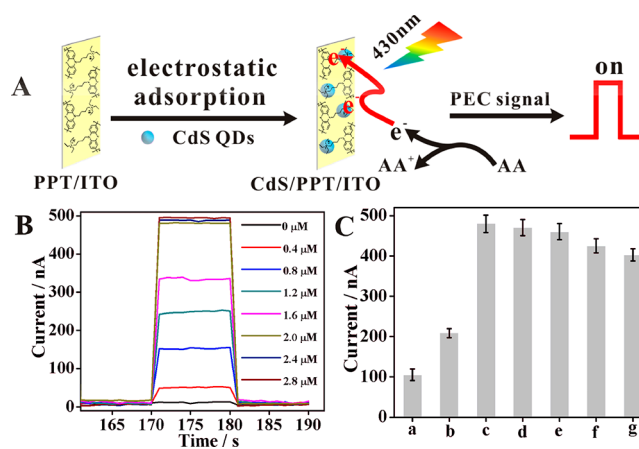


**Figure 2.** (A) Diagram of interaction of PPT/ITO and negatively charged CdS QDs. (B) PEC curves of PPT/ITO electrodes corresponding to different CdS QDs amounts. (C) PEC current intensities of different electrodes toward  $2.0\text{ }\mu\text{M}$  CdS QDs: (a) PDDA/ITO, (b) PT/ITO, (c) PPT/ITO fabricated from one CV scan, (d) PPT/ITO fabricated from two CV scans, (e) PPT/ITO fabricated from four CV scans, (f) PPT/ITO fabricated from six CV scans, and (g) PPT/ITO fabricated from eight CV scans.



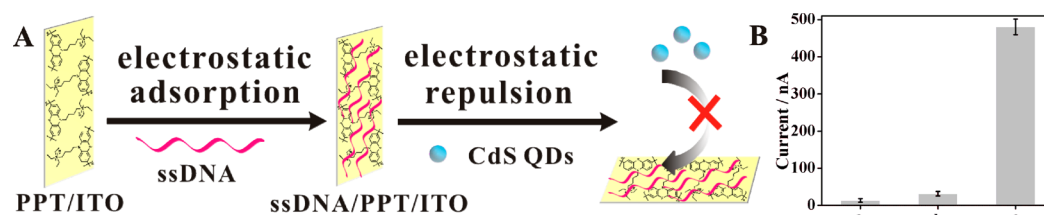


**Figure 3.** (A) Diagram of influence of ssDNA on the preparation of CdS/PPT/ITO electrode. (B) PEC current intensities of PPT/ITO electrodes under different conditions: (a) PPT/ITO, (b) ssDNA/PPT/ITO + CdS QDs, and (c) CdS/PPT/ITO.

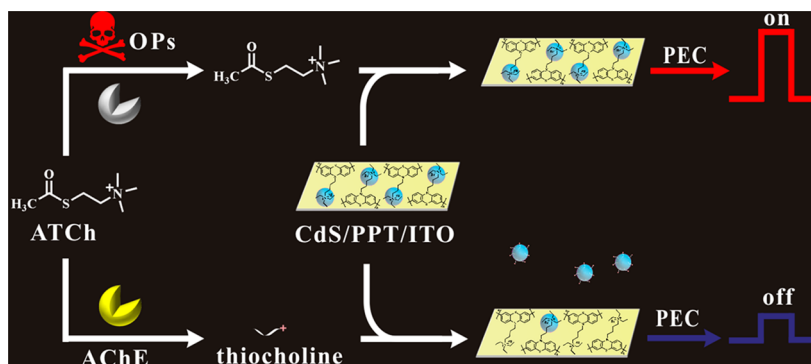


**Figure 4.** Diagram of the working principle for sensitive detection of OPs based on the CdS/PPT/ITO-based PEC sensor.

in PEC current was observed, arising from the saturated adsorption of CdS QDs on the PPT/ITO surface. Consequently,  $2.0 \mu\text{M}$  was used as the optimized concentration for CdS QDs to fabricate the electrode. In addition, reaction time was also investigated to sufficiently decorate CdS QDs on the PPT/ITO surface, and 30 min was chosen as the optimum time obtained from the unchanged PEC currents (Figure S8). To shed new light on the decoration of CdS QDs on the PPT/ITO surface, as illustrated in Figures S2E and Figure S5, XPS, SEM, and EDS characterizations of CdS/PPT/ITO were carried out, respectively. It is obvious that the image, XPS curve, and EDS curve of CdS/PPT/ITO displayed new nanoparticles (deemed as CdS QDs) and peaks (3.3 keV in EDS curve, and 405.24 and 412.46 eV in XPS curve, corresponding to Cd element) compared with that of PPT/ITO, implying the fact that CdS QDs were successfully anchored on the PPT/ITO surface.

To gain more insight into the fabrication of CdS/PPT/ITO, monomer PT, poly(dimethyldiallylammonium chloride) (PDDA), and phenothiazine polymeric films prepared from different CV scans (2, 4, 6, and 8) were applied for fabricating the photoelectrodes to explore the PEC performance (Figure 2C). After the immobilization of the CdS QDs, the spin-coated phenothiazine film possessed a PEC current of only 208.9 nA. In contrast, the phenothiazine polymeric films exhibited significantly enhanced PEC currents of 480, 470.6, 460.5, 425.6, and 402.9 nA, respectively, which are far greater than that of phenothiazine monomer in the spin-coated film state. In the phenothiazine polymeric film, the phenothiazine units are linked into film by C–C covalent bonds, and these linkages exposed more quaternary ammonium salt groups on the surface, which are conducive to immobilization of more CdS QDs, subsequently increasing the PEC current. In addition, the trend of reducing PEC current from one to eight CV scans implies that film deposition thickness is also crucial for enhancing PEC current, either to permit positive groups on the surface or to influence the conductivity. PDDA is one kind of

positively charged polymer and exhibits high solubility in water solution. When PDDA was used to replace phenothiazine polymer to immobilize CdS QDs, the fabricated electrode just demonstrated a very low PEC current of 105.1 nA. This firmly verified that the phenothiazine polymeric film not only provides abundant positive groups to adsorb CdS QDs but also works as an effective charge acceptor and transporter to enhance the separation of photogenerated charges, consequently improving the generation efficiency of PEC current.

To study the CdS-guided PEC current improvement phenomenon, the electrostatic adsorption of PPT/ITO toward CdS QDs was evaluated through the preincubation of negatively charged ssDNA with PPT/ITO and the subsequent addition of CdS QDs. The drawing scheme is depicted in Figure 3A. Evidently, ssDNA could cover the surface positive charges of PPT/ITO electrode via electrostatic adsorption, thus transforming the electrode from positive charge to negative charge. The surface negative charge helps ssDNA/PPT/ITO to prohibit the anchoring of CdS QDs on the PPT/ITO electrode due to electrostatic repulsion. As a result, the PEC current was not increased due to immobilization of no CdS QDs. The detailed experimental results are shown in Figure 3B. In comparison with the case where ssDNA was absent, preincubation of ssDNA with PPT/ITO led to a relatively low PEC current similar to that of PPT/ITO only, ascribed to the strong electrostatic adsorption of ssDNA and PPT/ITO, and strong electrostatic repulsion of ssDNA/PPT/ITO and CdS QDs.

**Analysis of OPs Based on the CdS/PPT/ITO-Based PEC Sensor.** Taking into account the aforementioned features, it was expected that the CdS/PPT/ITO electrode could be used as a popular PEC sensor to detect chemicals or biologics in a high-sensitivity manner. We demonstrated this hypothesis by soaking the photoelectrode in PBS buffer comprising OPs, ATCh, and AChE, followed by PEC measurement using AA as a sacrificial electron donor. OPs play an essential role in pest and disease control, but the

toxicities of OPs to humans and animals lead to dysfunctional AChE activity, subsequently resulting in neurodegenerative disorders. As a result, exploring a reliable assay for OP-sensitive biosensing is in high demand. The sensing mechanism for PEC detection of OPs is depicted in Figure 4. AChE catalyzed hydrolysis of ATCh into thiocholine, which competitively interacted with CdS QDs in CdS/PPT/ITO via the stronger Cd–S bonds compared with electrostatic binding, subsequently forming thiocholine-modified CdS QDs with abundant quaternary ammonium salt groups on the surface. As a consequence, CdS QDs fell from the PPT/ITO electrode due to electrostatic repulsion, and the PEC current was significantly reduced. Upon the preincubation of OPs with AChE, ATCh cannot be hydrolyzed into thiocholine because of the depressed AChE activity. Further, ATCh only has the thioether bond and quaternary ammonium salt group and consequently cannot wrest the CdS QDs from CdS/PPT/ITO via the formation of stronger chemical bonds.<sup>36–38</sup> In this context, PEC current would not be decreased.

To confirm the feasibility of the CdS/PPT/ITO-based PEC sensor for OP detection, several experiments in the absence/presence of OPs were carried out by using chlorpyrifos as a model OP (Figure 5A). Evidently, AChE or ATCh or

another validation experiment, the preincubation of chlorpyrifos with AChE brings about a significantly enhanced PEC response as compared with that of AChE alone. Furthermore, the PEC current value elevates along with the increased chlorpyrifos amounts, corresponding well to the principle that more chlorpyrifos would inhibit more AChE activity to generate thiocholine. On the basis of the PEC current change, it is completely feasible to detect OPs using the fabricated CdS/PPT/ITO photoelectrode.

#### Analytical Performance of CdS/PPT/ITO-Based PEC

**Sensor.** For the sake of getting a preeminent performance for the OP assay, AChE concentrations, ATCh concentrations, reaction time of AChE, ATCh, and CdS/PPT/ITO, and preincubation time of OPs and AChE that are directly related to the generation of thiocholine were investigated (Figure S9). Under the optimized conditions (AChE 14 mU/mL, ATCh 30  $\mu$ M, reaction time 35 min, and preincubation time 30 min), the analytical performance of the CdS/PPT/ITO-based PEC sensor was evaluated through testing PEC currents of the system comprising various chlorpyrifos amounts, and the experimental data are presented in Figure 5B. The PEC current kept increasing with the growing chlorpyrifos amounts from 1.5  $\mu$ g/L to 200  $\mu$ g/L, demonstrating an obviously positive relationship. To quantitatively assess the ability of the CdS/PPT/ITO-based PEC sensor for chlorpyrifos analysis, a working curve was plotted by employing PEC current ( $I$ ) and chlorpyrifos concentrations ( $C_{\text{chl}}$ ) as vertical and horizontal coordinates, respectively. The curve in Figure 5C implied that  $I$  was linearly relevant to chlorpyrifos amounts ranging from 1.5  $\mu$ g/L to 200  $\mu$ g/L. The linear equation was described as  $I = 1.606C_{\text{chl}} + 73.05$ , with a coefficient of 0.9899 and detection limit (LOD) of 0.63  $\mu$ g/L. The assay performances of our proposed sensor and other approaches for OPs are summarized in Table S1. The results demonstrated that the LOD was comparable or lower than that of previously reported methods, confirming the sufficiency of our sensor for OP biosensing. Furthermore, five different CdS/PPT/ITO electrodes were employed to detect chlorpyrifos (200  $\mu$ g/L), respectively. The relative standard deviations (RSDs) were calculated to be 1.78%, 2.03%, 1.52%, 2.75%, and 2.66%, respectively, which are within an acceptable range, implying good repeatability.

Selectivity was investigated due to its key role in assuring diagnosis accuracy and reducing misdiagnosis. According to the sensing principle, the CdS/PPT/ITO-based PEC sensor is only supposed to be responsive for AChE inhibitors. Thus, vitamin B, citric acid, glucose, dibrom, and omethoate were applied as interferences to verify the specificity and universality of the established PEC sensor for OPs (Figure 5D). Vitamin B or citric acid or glucose had little influence on the PEC current compared with that of the solution comprising AChE and ATCh due to their weak or no depression on AChE activity. In contrast, both dibrom and omethoate caused significant PEC current enhancement, corresponding well to the fact that dibrom and omethoate are OPs and can inhibit AChE activity with high efficiency. All of these results suggest that the CdS/PPT/ITO-based PEC sensor possesses good versatility for OP analysis and splendid selectivity for distinguishing OPs against other interfering biomolecules, providing a significant potential for application in real samples.

Further, the CdS/PPT/ITO-based PEC sensor was applied in the analysis of chlorpyrifos in cabbage extract and lake water obtained from Qingdao Agriculture University through the

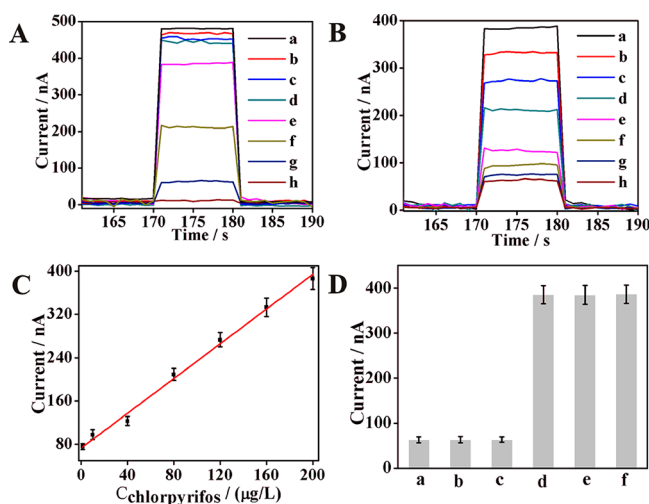


**Figure 5.** (A) PEC curves of the CdS/PPT/ITO-based sensor under different conditions: (a) CdS/PPT/ITO, (b) CdS/PPT/ITO + AChE, (c) CdS/PPT/ITO + ATCh, (d) CdS/PPT/ITO + chlorpyrifos, (e) CdS/PPT/ITO + AChE + ATCh + 200  $\mu$ g/L chlorpyrifos, (f) CdS/PPT/ITO + AChE + ATCh + 80  $\mu$ g/L chlorpyrifos, (g) CdS/PPT/ITO + AChE + ATCh, and (h) PPT/ITO. (B) PEC curves of the CdS/PPT/ITO-based sensor subjected to different chlorpyrifos concentrations: (a) 200, (b) 160, (c) 120, (d) 80, (e) 40, (f) 10, (g) 1.5, (h) 0  $\mu$ g/L. (C) Linear curve of PEC current intensities and chlorpyrifos concentrations. (D) PEC current intensities of the CdS/PPT/ITO-based sensor corresponding to different substances: (a) vitamin B, (b) citric acid, (c) glucose, (d) dibrom, (e) omethoate, (f) chlorpyrifos.

chlorpyrifos alone caused a slight change in PEC current compared with that of CdS/PPT/ITO. In contrast, when both AChE and ATCh are present, a remarkably decreased PEC current was recorded with a value of 63.04 nA. It came as no surprise to us that the hydrolysis product efficiently leads to the separation of CdS QDs and PPT/ITO, which can also be confirmed by the decreased XPS peak located at 405.24 and 412.46 eV corresponding to Cd element (Figure S2E). In

spiking method to explore its practical performance. The experiment was conducted by adding chlorpyrifos into cabbage extract and lake water at concentrations of 30  $\mu\text{g/L}$ , 60  $\mu\text{g/L}$ , and 100  $\mu\text{g/L}$ , followed by PEC measurement, and the results are summarized in Table S2. The CdS/PPT/ITO-based PEC sensor depicted recoveries in the range of 96.20–107.00% and low RSDs ranging from 2.78% to 6.86%. Moreover, the diagnosis results were also in accord with HPLC data. Therefore, the figures of merit implied that the CdS/PPT/ITO-based PEC sensor has been prosperously developed with excellent practical ability for assay of OPs in real samples.

## CONCLUSIONS

In summary, we have reported a versatile strategy to fabricate phenothiazine polymeric film on an ITO electrode (PPT/ITO) with fabulous stability and abundant quaternary ammonium salt groups that allow for electrostatic binding with functional materials, and we also presented their utilization in the development of a PEC sensor for target analyte detection. Due to the strong electrostatic adsorption of CdS QDs on the PPT/ITO electrode, the CdS/PPT/ITO-based PEC sensor was successfully developed with high PEC current under visible light irradiation. This character rendered it able to assay OPs present at approximately the ng/mL level in sensitivity and specificity. The applicability of the CdS/PPT/ITO-based PEC sensor for real sample determination was displayed by assaying chlorpyrifos spiked in cabbage extract and lake water. This strategy is widely applicable to many other substances with negative charges. Highly sensitive detection of other analytes can be readily achieved by varying the negatively charged substances, thus depicting a general PEC sensor for diverse biomolecule assay. We envisage that this work will provide new ideas for the fabrication of photoelectrodes with high photoelectric conversion efficiency and will introduce a new era in PEC sensing.

## ASSOCIATED CONTENT

### Supporting Information

The Supporting Information is available free of charge on the ACS Publications website at DOI: 10.1021/acs.analchem.9b03311.

Additional information as noted in the text. OP assay performance of the present strategy with other methods; recoveries for chlorpyrifos; Figures S1–S10 as described in the text (PDF)

## AUTHOR INFORMATION

### Corresponding Authors

\*Tel/Fax: 86-532-86080855. E-mail: lifeng@qau.edu.cn.

\*E-mail: lihaiyin@qau.edu.cn.

### ORCID

Feng Li: 0000-0002-3894-6139

### Notes

The authors declare no competing financial interest.

## ACKNOWLEDGMENTS

This work was funded by the National Natural Science Foundation of China (21605093 and 21775082), the Special Foundation for Distinguished Taishan Scholar of Shandong Province (ts201511052), and the Major Program of Shandong Province Natural Science Foundation (ZR2018ZC0127).

## REFERENCES

- (1) Barpuzary, D.; Kim, K.; Park, M. J. *ACS Nano* **2019**, *13*, 3953–3963.
- (2) Kumar, S.; Malik, T.; Sharma, D.; Ganguli, A. K. *ACS Appl. Nano. Materials* **2019**, *2*, 2651–2662.
- (3) Windle, C. D.; Kumagai, H.; Higashi, M.; Brisse, R.; Bold, S.; Jousselm, B.; Chavarot-Kerlidou, M.; Maeda, K.; Abe, R.; Ishitani, O.; Artero, V. J. *Am. Chem. Soc.* **2019**, *141*, 9593–9602.
- (4) Chang, J. F.; Wang, X.; Wang, J.; Li, H. Y.; Li, F. *Anal. Chem.* **2019**, *91*, 3604–3610.
- (5) Zhou, Y.; Shi, Y.; Wang, F. B.; Xia, X. H. *Anal. Chem.* **2019**, *91*, 2759–2767.
- (6) Cao, H. J.; Liu, S. S.; Tu, W. W.; Bao, J. C.; Dai, Z. H. *Chem. Commun.* **2014**, *50*, 13315–13318.
- (7) Li, Y.; Zhang, N.; Zhao, W. W.; Jiang, D. C.; Xu, J. J.; Chen, H. Y. *Anal. Chem.* **2017**, *89*, 4945–4950.
- (8) Dai, H.; Zhang, S. P.; Hong, Z. S.; Lin, Y. Y. *Anal. Chem.* **2016**, *88*, 9532–9538.
- (9) Zhu, H.; Hu, Y. F.; Zhu, K.; Yan, S. C.; Lu, L.; Zhao, M. M.; Fu, H. W.; Li, Z. S.; Zou, Z. G. *Chem. Commun.* **2018**, *54*, 11116–11119.
- (10) Hao, N.; Hua, R.; Chen, S. B.; Zhang, Y.; Zhou, Z.; Qian, J.; Liu, Q.; Wang, K. *Biosens. Bioelectron.* **2018**, *101*, 14–20.
- (11) Wang, H. H.; Li, M. J.; Wang, H. J.; Chai, Y. Q.; Yuan, R. *ACS Appl. Mater. Interfaces* **2019**, *11*, 23765–23772.
- (12) Liu, C. H.; Qiu, Y. Y.; Wang, F.; Wang, K.; Liang, Q.; Chen, Z. D. *Adv. Mater. Interfaces* **2017**, *4*, 1700681.
- (13) Zhao, K.; Yan, X. Q.; Gu, Y.; Kang, Z. S.; Bai, Z. M.; Cao, S. Y.; Liu, Y. C.; Zhang, X. H.; Zhang, Y. *Small* **2016**, *12*, 245–251.
- (14) Zeng, R. J.; Luo, Z. B.; Su, L. S.; Zhang, L. J.; Tang, D. P.; Niessner, R.; Knopp, D. *Anal. Chem.* **2019**, *91*, 2447–2454.
- (15) Bornoz, P.; Prevot, M. S.; Yu, X. Y.; Guijarro, N.; Sivula, K. J. *Am. Chem. Soc.* **2015**, *137*, 15338–15341.
- (16) Sick, T.; Hufnagel, A. G.; Kampmann, J.; Kondofersky, I.; Calik, M.; Rotter, J. M.; Evans, A.; Doblinger, M.; Herbert, S.; Peters, K.; Bohm, D.; Knochel, P.; Medina, D. D.; Fattakhova-Rohlfing, D.; Bein, T. *J. Am. Chem. Soc.* **2018**, *140*, 2085–2092.
- (17) Sun, H. J.; Neumann, C.; Zhang, T.; Löffler, M.; Wolf, A.; Hou, Y. L.; Turchanin, A.; Zhang, J.; Feng, X. *Adv. Mater.* **2019**, *31*, e1900961.
- (18) Zhang, P. S.; Wang, H.; Hong, Y. X.; Yu, M. L.; Zeng, R. J.; Long, Y. F.; Chen, J. *Biosens. Bioelectron.* **2018**, *99*, 318–324.
- (19) Zhao, Y.; Kamiya, K.; Hashimoto, K.; Nakanishi, S. *J. Mater. Chem. A* **2016**, *4*, 3858–3864.
- (20) Fernandez, E.; Rivero-Crespo, M. A.; Dominguez, I.; Rubio-Marques, P.; Oliver-Meseguer, J.; Liu, L.; Cabrero-Antonino, M.; Gavara, R.; Hernandez-Garrido, J. C.; Boronat, M.; Leyva-Perez, A.; Corma, A. *J. Am. Chem. Soc.* **2019**, *141*, 1928–1940.
- (21) Zhou, Y. B.; Wang, Y. Q.; Ning, L. C.; Ding, Z. C.; Wang, W. L.; Ding, C. K.; Li, R. H.; Chen, J. J.; Lu, X.; Ding, Y. J.; Zhan, Z. P. *J. Am. Chem. Soc.* **2017**, *139*, 3966–3969.
- (22) Yuan, L.; Franco, C.; Crivillers, N.; Mas-Torrent, M.; Cao, L.; Sangeeth, C. S. S.; Rovira, C.; Veciana, J.; Nijhuis, C. A. *Nat. Commun.* **2016**, *7*, 12066.
- (23) He, C. Y.; Fan, S. L.; Zhang, X. G. *J. Am. Chem. Soc.* **2010**, *132*, 12850–12852.
- (24) Puthongkham, P.; Lee, S. T.; Venton, B. J. *Anal. Chem.* **2019**, *91*, 8366–8373.
- (25) Luo, S. C.; Sekine, J.; Zhu, B.; Zhao, H. C.; Nakao, A.; Yu, H.-h. *ACS Nano* **2012**, *6*, 3018–3026.
- (26) Bhattacharjya, D.; Mukhopadhyay, I. *Langmuir* **2012**, *28*, 5893–5899.
- (27) Bai, S.; Hu, Q.; Zeng, Q.; Wang, M.; Wang, L. *ACS Appl. Mater. Interfaces* **2018**, *10*, 11319–11327.
- (28) Gu, C.; Huang, N.; Wu, Y.; Xu, H.; Jiang, D. L. *Angew. Chem., Int. Ed.* **2015**, *54*, 11540–11544.
- (29) Liu, J.; Zhao, X.; Al-Galiby, Q.; Huang, X.; Zheng, J.; Li, R.; Huang, C.; Yang, Y.; Shi, J.; Manrique, D. Z.; Lambert, C. J.; Bryce, M. R.; Hong, W. *Angew. Chem., Int. Ed.* **2017**, *56*, 13061–13065.

- (30) Li, H. Y.; Wang, C. F.; Hou, T.; Li, F. *Anal. Chem.* **2017**, *89*, 9100–9107.
- (31) Li, H. Y.; Chang, J. F.; Gai, P. P.; Li, F. *ACS Appl. Mater. Interfaces* **2018**, *10*, 4561–4568.
- (32) Blanco, G. D.; Hiltunen, A. J.; Lim, G. N.; Kc, C. B.; Kaunisto, K. M.; Vuorinen, T. K.; Nesterov, V. N.; Lemmetyinen, H. J.; D'Souza, F. *ACS Appl. Mater. Interfaces* **2016**, *8*, 8481–8490.
- (33) Lu, C.; Paramasivam, M.; Park, K.; Kim, C. H.; Kim, H. K. *ACS Appl. Mater. Interfaces* **2019**, *11*, 14011–14022.
- (34) Chen, Y. C.; Kuo, Y. T.; Liang, C. J. *RSC Adv.* **2018**, *8*, 9783–9789.
- (35) Zhang, L.; Hao, Y. Q.; Wang, X. Y.; Long, Y. F.; Ramos, A.; Jiang, D. L.; Ma, X. H.; Lin, Q. L.; Zhou, F. M. *Electroanalysis* **2015**, *27*, 1899–1905.
- (36) Duran, G. M.; Contento, A. M.; Rios, A. *Anal. Chim. Acta* **2013**, *801*, 84–90.
- (37) Wang, J.; Yan, Y.; Yan, X.; Hu, T. Y.; Tang, X. J.; Su, X. G. *Sens. Actuators, B* **2016**, *234*, 470–477.
- (38) Yan, X.; Li, H.; Li, Y.; Su, X. *Anal. Chim. Acta* **2014**, *852*, 189–195.